Heliyon 9 (2023) e16775

Contents lists available at ScienceDirect

Heliyon

journal homepage: www.cell.com/heliyon

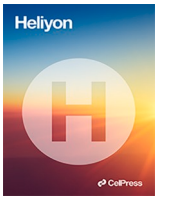

Emission properties of Pd-doped $CsPbBr_3$ perovskite nanocrystal: Infrared emission due to the Pd-doping

Mabel Rodríguez-Fernández [a], José Carlos Piñero [b], Rodrigo Alcántara [a], Juan Jesús Gallardo [a], Javier Navas [a,*]

[a] Department of Physical Chemistry, University of Cádiz, E-11510, Puerto Real, Spain
[b] Department of Didactics (Area of Maths), University of Cádiz, E-11510, Puerto Real, Spain

ARTICLE INFO

Keywords:
Luminescence
Perovskite
Nanocrystals
Sensors

ABSTRACT

Perovskite-type materials have attracted great attention in recent times due to their interesting characteristics, such as their luminescent properties. The good photoluminescence quantum yields as well as the possibility of tuning the emission wavelength has allowed the study of these materials in several applications, such as sensors or LEDs. As sensors, making nanocrystals of these perovskites emitting in the near infrared (NIR) would open the possibility of using these materials in biomedical applications. In the present work, Pd-doped $CsPbBr_3$ perovskite nanocrystals (NCs) were synthesized and characterized. We show here Pd-doped NCs synthesized emit in NIR, at about 875 nm, using a laser emitting at 785 nm as the excitation source. This result is really new and promising, because it opens the possibility of using these nanocrystals in many applications as sensor in the field of nanobiomedicine in the future.

1. Introduction

Perovskite nanomaterials with an ABX_3 structure in which A is a monovalent inorganic or organic cation, B a divalent inorganic cation and X a halogen anion have recently emerged as promising nanomaterials due to their excellent optoelectronic properties. These have attracted considerable attention for their applications in devices including light-emitting diodes (LEDs) [1], lasers [2], photodetectors [3], sensors [4] and solar cells [5,6].

Currently, the study of quantum dots (QDs) and nanocrystals (NCs) based on perovskite materials has attracted great attention due to their interesting properties derived from quantum size effects, such as the possibility of controlling the optical band gap [7], the high mobility of carriers [8] or the possibility of tuning the photoluminescent emission across the entire spectrum [9]. Thus, completely inorganic perovskites based on caesium and lead have shown interesting properties that make them very interesting in the aforementioned applications, such as stable emission in the visible [10], or long lifetimes [11].

In this sense, one of the applications of greatest interest for luminescent materials is their use as sensors in several topics, but they have acquired special relevance in the field of biomedicine, and specifically in temperature detection, due to the high sensitivity of the variation of the luminescent properties, intensity or bandwidth, with temperature. It enables accurate and remote thermal sensing in real time for medical applications such as the early diagnosis of tumours and hyperthermia [12]. But, for this application, the emission and excitation bands should be within the any of the three biological windows (BW–I: 650–950 nm, BW-II: 1000–1350 nm and BW-III:

* Corresponding author.
E-mail address: javier.navas@uca.es (J. Navas).

https://doi.org/10.1016/j.heliyon.2023.e16775
Received 27 February 2023; Received in revised form 26 May 2023; Accepted 26 May 2023
Available online 27 May 2023

1550–1870 nm) [13]. Therefore, the search for materials capable of absorbing and emitting in these areas of the spectrum, that is, in the near infrared (NIR), is of great interest. Therefore, the possibility of designing QDs or NCs based on perovskites but with NIR emission would be of great interest because it would open the possibility of using these materials in in vivo temperature detection in biomedical applications. Strategies such as perovskite doping have been used in the past to control their emission properties, so it may be an interesting way to design NIR-emitting perovskites.

Perovskite doping in "B" and "X" positions allows for control over the emission and excitation wavelength in perovskite quantum dots [14,15], which could fall in the first biological window. Several works have shown the doping in B position using different dopants. For example, Zhu et al. showed an increase in the photoluminescence quantum yield in Dy-doped $CsPbBr_3$ perovskite [16]. Ding et al. reported up-conversion process in $CsPbF_3$: Zn^{2+}-Yb^{3+}-Tm^{3+} (or Er^{3+}) perovskite nanocrystals (PeNCs)/Au nanorods (NRs) array hybrid [17]. Tri-doping of $CsPbCl_3$ using Cr^{3+}, Yb^{3+} and Ce^{3+} have shown excellent quantum yield and stability [18]. Zhang et al. reported Sr-doped $CsPbBr_3$ perovskite in which the emission wavelength could be tunned due to the doping [19]. Ding et al. showed that optoelectronic properties and stability of $CsPbI_3$ PQDs are significantly improved by Er^{3+} doping [20]. Co-doping enhanced the photocatalytic activity of $CsPbBr_3$ for hydrogen production [21]. In addition, in previous work, we demonstrated that doping with Pd of $MAPbI_3$ (where MA^+ corresponds to the methylammonium cation) leads to a decrease in the band-gap value [22]. However, inorganic perovskite such as $CsPbBr_3$ is more stable than hybrid organic-inorganic perovskite such as $MAPbI_3$ [23].

In this work, a two-part study was performed into the photoluminescent emission of perovskite nanocrystals. First, a study was performed into the influence of the Pd-doping in B-site in the $CsPbBr_3$ perovskite structure and photoluminescent emission. To this aim, perovskite nanocrystals with an $CsPb_{1-x}Pd_xBr_3$ composition ($x = 0.25$) were synthesized using a hot-injection method. For choosing this Pd concentration, several $CsPb_{1-x}Pd_xBr_3$ perovskites in bulk form changing the x values were synthesized and the crystalline structure was analysed by x-ray diffraction in order to know the Pd concentration in which the perovskite structure was obtained. From this analysis, a x value of 0.25 was defined as the adequate Pd concentration for preparing the perovskite NCs. In addition, Pd was chosen because a decrease in the band gap in Pd-doped perovskite has been reported [22], thus an emission falling in the first biological window can be expected, which is typically reported for the doping using rare earths ions, in addition to the typical emission of $CsPbBr_3$ NCs in the green zone of the electromagnetic spectrum [24]. Secondly, the effect of the reaction temperature on the structure and photoluminescent emission properties of pure and doped perovskite NCs was also analysed. To this end, the NCs with the aforementioned composition were synthesized at four different temperatures: 130 °C, 150 °C, 170 °C and 190 °C.

2. Material and methods

2.1. Reagents

Caesium carbonate (Cs_2CO_3, 99.5% trace metals basis), lead(II) bromide ($PbBr_2$, $\geq$ 98%), palladium(II) bromide ($PdBr_2$, 99%) oleylamine (OLA, technical grade 70%), oleic acid (OA, technical grade 90%), 1-octadecene (ODE for synthesis), toluene anhydrous (99.8%), dimethyl sulfoxide (DMSO, $\geq$ 99.5%) and caesium bromide (CsBr, 99.9%) were supplied by Sigma-Aldrich©.

2.2. Synthesis of Pd-doped $CsPbBr_3$ NCs

Synthesis $CsPb_{1-x}Pd_xBr_3$ perovskite bulk. First, it was necessary to determine the amount of Pd with which it was possible to dope the $CsPbBr_3$ while maintaining the perovskite structure. To this end, $CsPb_{1-x}Pd_xBr_3$ perovskite bulks (where $x = 0$, 0.25, 0.5, 0.75, 1) were synthesized following the method employed by Ding et al. with some modifications [25]. Thus, $2.48{\cdot}10^{-3}$ mol of CsBr and $2.48{\cdot}10^{-3}$ mol of $PbBr_2$ were dissolved in 2 mL DMSO in an ultrasound bath and then the mixture was heated on a hot plate at 60 °C until powders of the undoped $CsPbBr_3$ perovskite were obtained. For the doped perovskite, the amount of $PbBr_2$ was modified by adding the stoichiometric amount of $PdBr_2$ to obtain the aforementioned composition of $CsPb_{1-x}Pd_xBr_3$ perovskites.

Preparation of Cs-Oleate. The synthesis procedure was based on a previously reported method [26]. Cs-oleate was obtained by loading 0.814 g of Cs_2CO_3, 40 mL of ODE and 2.5 mL of OA into a 100 mL 3-neck flask, drying the mixture for 1 h at 120 °C under vacuum. Next, the mixture was heated under N_2 atmosphere at 150 °C on a hot plate to ensure that all the Cs_2CO_3 reacted with the OA.

Synthesis of Pd-doped $CsPbBr_3$ NCs. From the results of the bulk doped perovskite, $CsPb_{1-x}Pd_xBr_3$ nanocrystals were synthesized, x being 0.25. This doping level allows internally Pd-doped perovskites to be obtained. The methodology followed to obtain Pd-doped $CsPbBr_3$ NCs was the hot-injection method described by Protesescu et al. [26], in which 0.141 mmol of $PbBr_2$ and 0.047 mmol of $PdBr_2$ in 5 mL of ODE was dried under vacuum for 1 h at 120 °C. A total of 0.5 mL of OLA and 0.5 mL of OA were injected at 120 °C under N_2 on a hot plate. Once the salt was dissolved, the temperature was increased to the desired synthesis temperature (130 °C, 150 °C, 170 °C or 190 °C) and 0.4 mL of Cs-oleate was injected before the flask was immediately immersed in an ice-water bath. Finally, the above dispersion underwent centrifugation at 7000 rpm for 10 min at 0 °C. For comparison purposes, undoped $CsPbBr_3$ NCs were synthesized following the same procedure, but adding the stoichiometric amount of $PbBr_2$ in the first step of the synthesis. On the other hand, the supernatant was discarded and the precipitate was dispersed in anhydrous toluene and taken as the colloidal suspension of perovskite nanocrystals.

2.3. Characterization of bulk and perovskite NCs samples

First, the doped perovskite bulk was characterized to observe whether the perovskite structure was formed for the different amounts of Pd tested. For this, the XRD patterns of the powder samples were obtained using a D8 Advance A-25 diffractometer with a

Lynxeye detector supplied by Bruker® with a Cu-Kα X-ray source. The patterns were recorded from 10° to 75° with a resolution of 0.020°, 40 kV and 40 mA.

Furthermore, the structural characterization of the PQD samples was performed by means of transmission electronic microscopy (TEM). The TEM and HR-TEM images of the samples were obtained using a Talos F200s X Twin transmission electron microscope supplied by ThermoFisher Instruments®, with an electron beam energy of 200 keV, an extraction voltage of 3900 V and an emission current of 65.1 μA. The element distributions of the samples were investigated using high-angle annular dark-field scanning transmission electron microscopy (HAADF-STEM) images coupled with the corresponding energy dispersive X-ray spectrometry (EDS) elemental mapping. The optical properties of the colloidal suspensions obtained from the perovskite NCs samples were determined using UV–Vis spectroscopy in absorbance mode by means of a modular equipment assembled in our laboratory consisting of a DH-2000-BAL light source and USB2000+ general purpose spectrometer, both supplied by OceanOptics©. Hellma Analytics™ supplied glass spectrophotometer cuvettes (model 100-10-20) with a 10 mm light path. Two different references were used: anhydrous toluene in the case of $CsPbBr_3$ perovskite NCs and ODE in the case of the Pd-doped samples. Finally, the emission properties of the samples were studied using photoluminescence spectroscopy. The steady-state photoluminescence spectra were recorded at room temperature with a Horiba© LabRAM HR Evolution modular Raman spectrometer, which is suited for both Raman analysis and photoluminescence, and is equipped with a Symphony II IR detector and a Sincerity visible detector both supplied by Horiba©. As excitation sources, different lasers were used: a He–Cd laser emitting at 325 nm (model IK3201R–F 25 mW supplied by Kimmon Koha©); two diode pumped solid state (DPSS) lasers emitting at 473 and 532 nm with a power output of 100 mW supplied by Quantum models©; a He–Ne laser, supplied by Pacific LasertecTM, with an emission at 633 nm; and a Sacher Lasertechnik© laser emitting at 785 nm (model Pilot PC 500, power output: 100 mW).

Time-resolved photoluminescence measurements for estimating the lifetime of the emissions were performed using a DeltaFlex Modular Fluorescence Lifetime System supplied by Horiba© and a 467 nm nanoLED (pulse duration <200 ps) as the excitation source.

3. Results and discussion

3.1. $CsPb_{1-x}Pd_xBr_3$ perovskite bulk

The crystalline configuration of $CsPb_{1-x}Pd_xBr_3$ (x = 0, 0.25, 0.5, 0.75, 1) perovskite bulk was analysed by XRD. Fig. 1 shows the

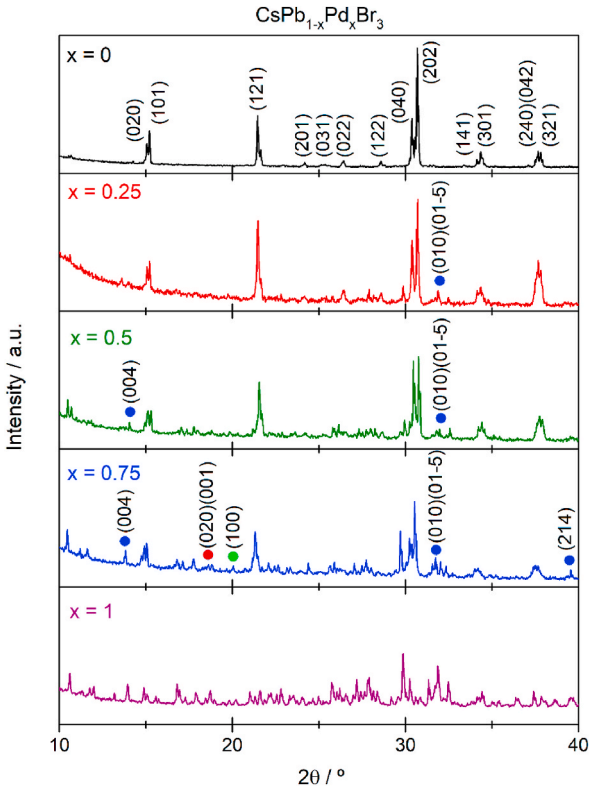

Fig. 1. Diffractograms of $CsPb_{1-x}Pd_xBr_3$ perovskite bulk, x = 0, 0.25, 0.5, 0.75, 1. The planes pointed out for the diffractogram with x = = are assigned to orthorhombic *Pnma* perovskite, planes with a blue circle for $PdBr_2$ monoclinic $P2_1/c$, a red circle for $PbBr_2$ orthorhombic *Pnma* and a green circle for CsBr cubic Pm-3m (PDF#73–0391). (For interpretation of the references to colour in this figure legend, the reader is referred to the Web version of this article.)

diffractograms of the samples obtained. The crystalline structure of $CsPbBr_3$ was confirmed to be orthorhombic *Pnma*, as suggested by the literature [27]. To make the assignation of the peaks more comprehensible, we have assigned the perovskite peaks in the diffractogram corresponding to $CsPbBr_3$ NCs, while in the others we have marked the new peaks corresponding to the precursors as follows: a blue circle for $PdBr_2$ monoclinic $P2_1/c$ (PDF#48–1715), a red circle for $PbBr_2$ orthorhombic *Pnma* (PDF#84–1181) and a green circle for CsBr cubic Pm-3m (PDF#73–0391). The *Pnma* orthorhombic perovskite structure typical for $CsPbBr_3$ remains until the composition $x = 0.5$, but some peaks corresponding to $PdBr_2$ start to appear when $x = 0.25$, which means that the Pd is not entering the perovskite structure completely, and a certain mixture of phases is observed. For $x = 0.75$, we can see mainly the peaks assigned to the precursors ($PbBr_2$, $PdBr_2$ and CsBr) and only a few are typical of the perovskite structure, which means that the perovskite was not successfully synthesized. Hence, we decided to synthesize perovskites NCs using $x = 0.25$ to be sure of their internal Pd doping. Undoped $CsPbBr_3$ NCs were also prepared to analyse the effect of Pd doping on their properties.

3.2. Perovskite NCs in colloidal suspension

3.2.1. Selected area diffraction (SAED) analysis

To explore the crystalline configuration of the different samples of the perovskite NCs in suspension, Bright Field (BF) TEM images were acquired and, as the nanoparticles were randomly oriented, a search for well-aligned nanoparticles (with respect to the incident beam) was conducted. Some of the nanoparticles showed an orientation that allows for a selected area diffraction pattern (SAED) study. In this regard, Fig. 2a shows TEM BF micrography of the $CsPbBr_3$ nanoparticles annealed at 170 °C. The nanoparticles are "square-shaped", conforming a structure that is similar to a square-based prism with 20 nm edges. Some of them are partially oriented with respect to the incident beam, while some others were aligned enough to perform the analysis. To distinguish "well-aligned nanoparticles", HREM images were acquired for a variety of nanoparticles (see Fig. 2b as an example). A nanoparticle was considered to be well-aligned when atomic columns could be appreciated and the fast Fourier transform (FFT) showed a comprehensible pattern.

Focusing on the $CsPbBr_3$ annealed at 170 °C, this sample is expected to form an orthorhombic lattice, belonging to the *Pnma* space group [28]. Thus, $CsPbBr_3$ in an orthorhombic configuration is expected to elongate along c-axis or [001] crystallographic axis. Therefore, there are always (*hk*0) diffractions forming an (*hk*0) reciprocal lattice row as a distinctive layer line in a SAED pattern. Taking this into consideration and once the camera constant (which depends on the observation conditions) is determined, d-spacing can be calculated as $d_{hkl} = \frac{\lambda \cdot L}{r}$, where $\lambda \cdot L$ is the camera constant (measured in Å·pixel), d_{hkl} is the d-spacing (in Å) and r is the geometric distance between the two adjacent SAED spots (here, measured in pixels). As the geometric distance between two SAED spots corresponds to the d-spacing between these two reciprocal lattice spots (which represent two adjacent parallel lattice planes in a real crystal lattice), measuring on the corresponding SAED (see Fig. 2c), makes it possible to determine d_{hk0} interplanar distances. On the other hand, in SAED patterns, each diffraction spot or reciprocal lattice point represents a set of equally spaced real lattice planes. Thus, measuring the angle between the (*hk*0) and (hkl) layer lines represented by dashed lines in Fig. 2c, the angle between the corresponding real lattice planes can be obtained. By using these data and the L/M relation presented in Fig. 2c, the [010] pole of an orthorhombic system is determined. This is in agreement with the literature [28] and with the fact that a *Pnma* space group permits only $h = 2n$ diffractions for (*hk*0) and $(k + l) = 2n$ for (0 *kl*). Thus, sample $CsPbBr_3$ 170 °C is coincident with a $CsPbBr_3$ in orthorhombic configuration with lattice parameters: $a = 8.87$ Å, $b = 8.84$ Å and $c = 11.98$ Å.

Regarding the $CsPb_{0.75}Pd_{0.25}Br_3$ perovskite NCs samples, some morphological changes are detected. Indeed, the samples annealed at 130 °C show nanoparticles (NP) with a hexagonal section that can be considered to be a circle with a diameter of approximately 20 nm. These NPs are accompanied by smaller ones with a circular section of 5 nm radius (see Fig. 3a). Unfortunately, no NPs were found well-aligned with the e-beam, so no HREM or SAED data could be presented here. The above-mentioned case can be compared with that of $CsPb_{0.75}Pd_{0.25}Br_3$ annealed at 190 °C. Fig. 3b shows BF micrography of such NPs. It can be observed that NPs were obtained with a square-based section. A white-dashed square is used in Fig. 3b to indicate the nanoparticle where the study was conducted. The inset in Fig. 3b shows the HREM imaging of the highlighted particle in Fig. 3b, and thus the interplanar distance in the random oriented

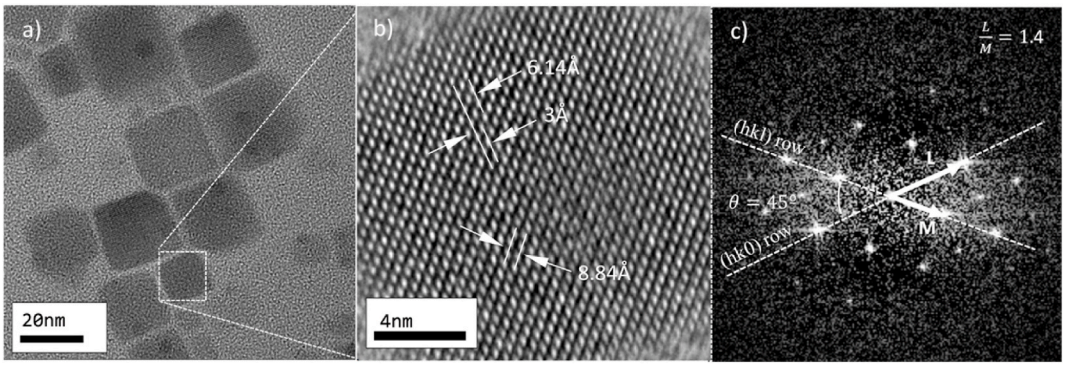

Fig. 2. TEM BF micrography of $CsPbBr_3$ nanoparticles synthesized in colloidal suspension (a) annealed at 170 °C, dashed-square indicates the particle where the SAED analysis was performed. Interplanar distances can be measured directly in the HREM image (b), and can be used to confirm the results obtained by indexing the SAED pattern (c).

NP can be directly measured. SAED image of the corresponding NP is shown in Fig. 3c. However, as the diffraction pattern was so complex, white dots with black edges were included to guide the eyes through the pattern. Our explanation for this phenomenon is that these NPs could be composed of a variety of domains [28], which induces some strain relaxation in the lattice, also due to the significant lower ionic radius of Pd^{2+} with respect to Pb^{2+}. An orthorhombic configuration is detected with lattice parameters: a = 8.89 Å, b = 8.82 Å and c = 12.08 Å. These results are quite similar to those obtained in the original $CsPbBr_3$ samples.

3.2.2. TEM analysis and size distribution

Fig. 4 shows representative TEM images of the undoped NCs synthesized in colloidal suspension at 130 °C (Figs. 4a), 150 °C (Figs. 4b), 170 °C (Fig. 4c), and 190 °C (Fig. 4d). Also, Fig. 5 shows Pd-doped NCs synthesized in colloidal suspension, at 130 °C (Figs. 5a), 150 °C (Figs. 5b), 170 °C (Fig. 5c), and 190 °C (Fig. 5d). From these TEM images, the size distributions of the samples were estimated, shown in Figs. S1 and S2 in the Supplementary Material. Statistical analysis of the size distributions reveals the average particle size of the samples, shown in Table 1.

As mentioned above, we employed the hot-injection method to grow the nanocrystals and their growth was mainly controlled by precisely setting the hot injection temperature to 130, 150, 170 and 190 °C. In general, the values of the average particle size show that the average size of NCs gradually increases as the temperature rises. In the case of the doped NCs, the samples prepared at 130, 150 and 170 °C were of a similar size, and the differences are in the order of accuracy. The sample prepared at 190 °C is clearly observed to increase in size. Furthermore, those values also demonstrate that the particle size decreases when the perovskite nanocrystals are doped with Pd, maybe because the crystallinity is worse for the doped samples, and those perovskite NCs grew less.

3.2.3. HAADF-STEM and EDS analysis

The element distributions of the samples were investigated using the high-angle annular dark-field scanning transmission electron microscopy (HAADF-STEM) image coupled with the corresponding energy dispersive X-ray spectrometry (EDS) elemental mapping. Fig. 6a shows the HAADF-STEM image of $CsPbBr_3$ NCs and Fig. 6a–d shows the corresponding EDS elemental mapping images of Cs, Pb, and Br elements for the sample synthesized at 130 °C, which is considered representative of all the samples synthesized. Also, Fig. 6e shows the Pd-doped NCs and Fig. 6f–i shows the corresponding EDS elemental mapping images of Cs, Pb, Br and Pd elements for the sample synthesized at 130 °C, which is also considered representative of all the samples synthesized. In the case of pristine $CsPbBr_3$ NCs, the elements show dense elemental profiles and seem dispersed around the sample, as Fig. 6a shows. This is due to the fact that this technique is not very sensitive to elements which have a low atomic number. For elements with a higher atomic number, more electrons are scattered at higher angles due to the presence of more intense electrostatic interactions between the nucleus and the electron beam. As a result, the HAADF detector senses a greater signal from atoms with a high Z [29]. For Pd-doped NCs, the Pd elemental profile appears to be concentrated in certain areas, the brighter ones, and also Pb appears to be concentrated in the same zones as Pd. In these zones, we can clearly observe perovskite NCs in the HAADF-STEM (see Fig. 6b). Thus, we can confirm the presence of Pb and Pd in the same particles, so this is indirect evidence of the internal doping of the perovskite NCs.

3.2.4. UV–Vis spectroscopy

UV–Vis spectra were recorded for the undoped and Pd-doped NCs synthesized in colloidal suspension. The spectra in Fig. 7a and b shows a broad band due to light dispersion phenomena. When the synthesis temperature decreases (and the particle size is smaller), a blue-shift is recorded at the edge of the extinction plot for both the doped and undoped perovskite NCs. That is consistent with the information found in the bibliography, in which it was found that the absorption edge is blue-shifted due to an increase of the quantum confinement effect [30]. These results also show that the effect of the Pd doping is a shift in the absorption edge towards higher energy values, i.e. lower wavelength, as is shown in the inset of Fig. 7a. Thus, by changing the synthesis temperature and doping with palladium, it is possible to modify the optical properties of the perovskite NCs. On the other hand, despite the broad band due to the

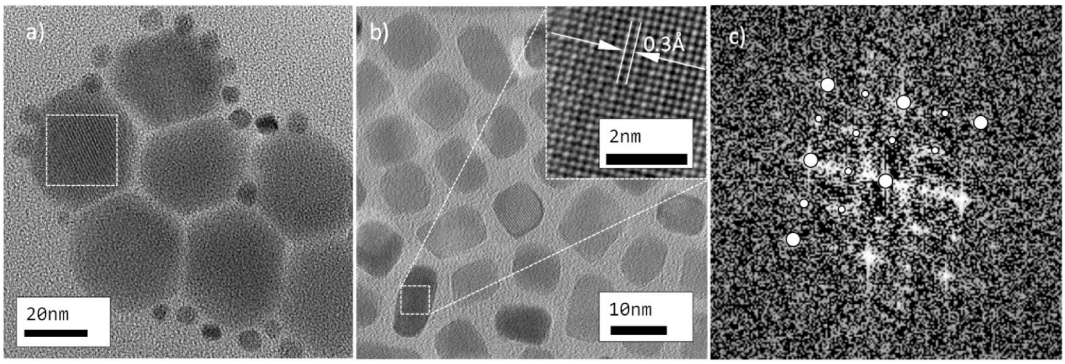

Fig. 3. TEM BF micrography of a) $CsPd_{0.75}Pd_{0.25}Br_3$ nanoparticles annealed at 130 °C, which show two types of NPs and hexagonal section. (b) TEM BF micrography of $CsPb_{0.75}Pd_{0.25}Br_3$ nanoparticles annealed at 190 °C, a square-like shape being observed. Inset shows HREM imaging of a selected NP, where interplanar distances could be measured. c) SAED data of the highlighted NP, showing a complex pattern that is attributed to a multi-domain structure that might relax strains in the crystal lattice.

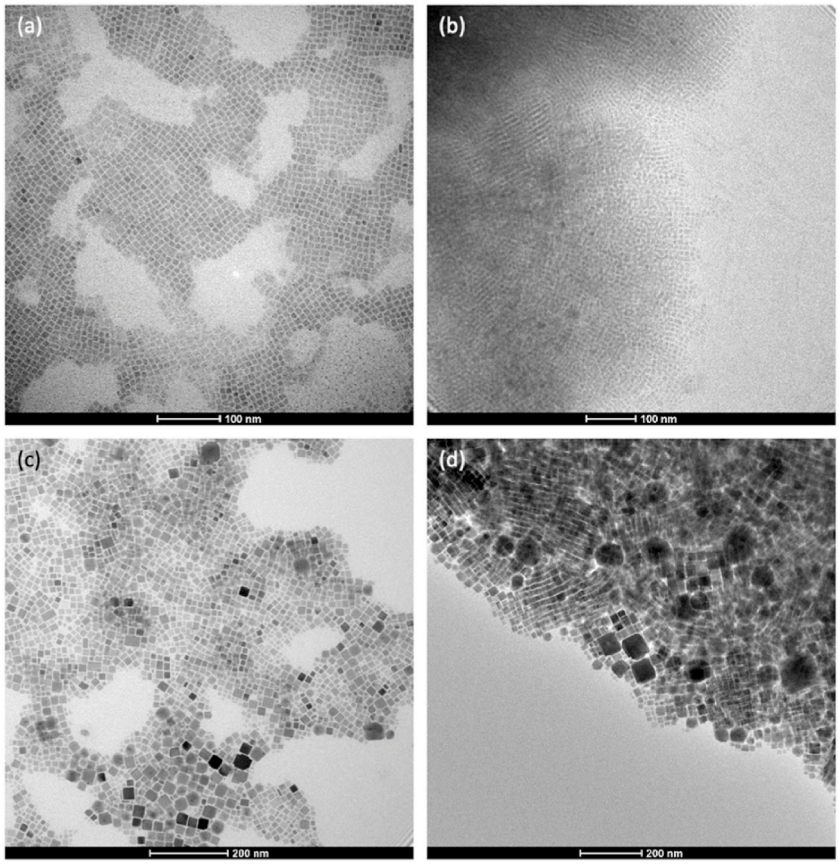

Fig. 4. TEM images of $CsPbBr_3$ NCs synthesized in colloidal suspension at 130 °C (a), 150 °C (b), 170 °C (c) and 190 °C (d).

scattering process, the first two exciton transitions are clearly observed in the undoped perovskite NCs with low size. These transitions are pointed out using an asterisk in Fig. 7a. But, these two transitions are not well-resolved for doped samples, which is due to a weak confinement in doped perovskite NCs [22].

3.2.5. *Photoluminescence spectroscopy*

Photoluminescence spectroscopy was employed to determine the effect of the synthesis temperature and Pd doping on the emission properties of the perovskite NCs. First, the effect of the synthesis temperature was studied. Fig. 8a shows the normalized spectra of the undoped perovskite NCs synthesized at different temperatures under excitation at $\lambda = 473$ nm. This band corresponds to the main emission of the $CsPbBr_3$ nanocrystals, which suffers a red-shift as the temperature increases, with the shift more noticeable from 130 to 150 °C, from 507 to 515 nm. The shift for the higher temperatures is negligible. This same effect can be observed as the synthesis temperature increases in the case of the Pd-doped samples, as is observed in Fig. 8b. Again, the more remarkable shift is produced between 130 and 150 °C, at about 9 nm, the differences between the emission at higher temperatures also being negligible.

Furthermore, we analysed the effect of Pd doping on the emission properties. Fig. 8c shows the photoluminescence spectra of the undoped (black) and Pd-doped NCs (red) at every synthesis temperature obtained under excitation at 473 nm. Comparing the photoluminescence spectra of the doped and undoped samples at the same synthesis temperature and under the same excitation wavelength, we can see that the effect of Pd doping is a blue shift of the main emission band, the shift being in the 14–16 nm range for the samples synthesized. This is coherent with the results obtained from UV–Vis spectroscopy. Using the laser emitting at 325 nm, similar results to those shown for the laser at 473 nm were found, as is observed in Fig. S3 in the Supplementary Material. The undoped and doped samples do not show emission using lasers emitting at 532 and 633 nm.

3.2.6. *Time-resolved photoluminescence spectroscopy*

Time-resolved photoluminescence spectroscopy was performed to obtain the average lifetime for the main emission shown in Fig. 8 for the undoped and Pd-doped samples. Fig. 9a and b shows the time-resolved PL decays for the undoped and Pd-doped NCs, respectively, which were fitted by a tri-exponential function, and the average lifetime was estimated. Details of this fitting and calculation are shown in the Supplementary Material. We can observe how the average lifetime is about 2 ns lower for the doped samples than for the undoped perovskite NCs, whose average lifetime is about 4 ns. These findings are similar to those reported in the literature [18], suggesting the excellent Stokes emission characteristics [18]. In detail, the average lifetime decreases with temperature

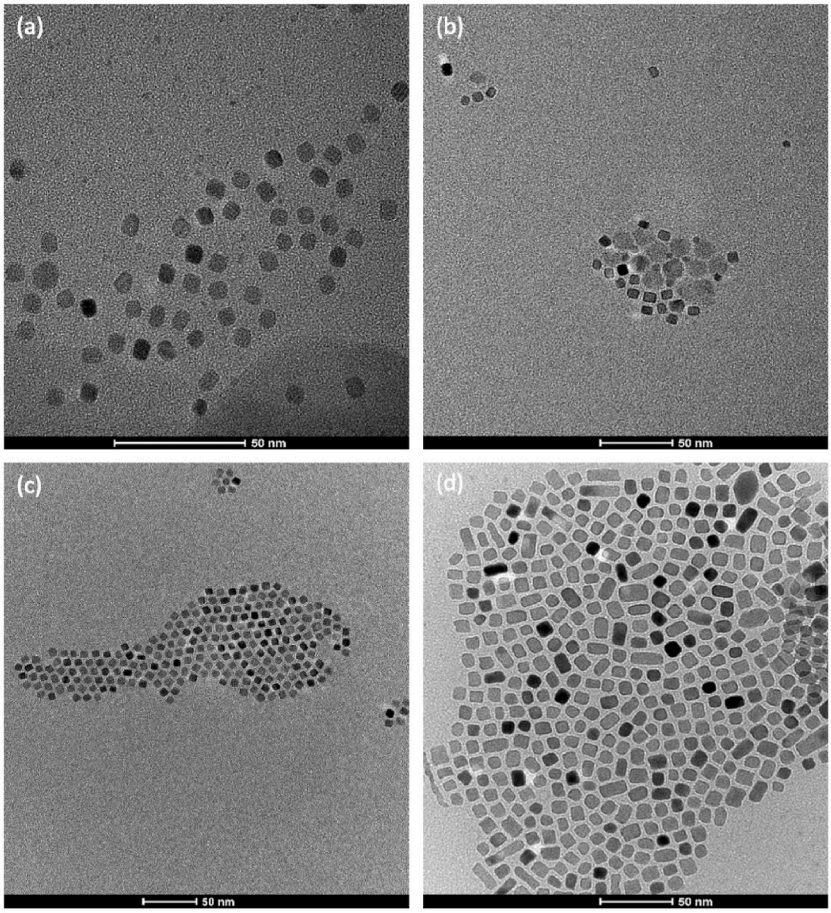

Fig. 5. TEM images of $CsPb_{0.75}Pd_{0.25}Br_3$ NCs synthesized at 130 °C (a), 150 °C (b), 170 °C (c) and 190 °C (d).

Table 1
Average particle size of the perovskite NCs synthesized in colloidal suspension.

T/°C	average size/nm	
	$CsPbBr_3$ NCs	Pd-doped $CsPbBr_3$ NCs
130	7.6 ± 1.2	6.3 ± 0.6
150	8.4 ± 1.3	7.0 ± 1.1
170	14.7 ± 4.5	6.8 ± 0.6
190	18.2 ± 5.2	10.0 ± 3.2

for the doped perovskite. The hot injection method used in this work uses hot solvent. The high temperature of the solvent promotes the formation of the quantum dots by driving the reaction forward quickly. However, this rapid synthesis process can result in defects and impurities within the quantum dots, which can act as non-radiative recombination centres for the excited charge carriers. At higher synthesis temperatures, the defects and impurities within the quantum dots become more prevalent, leading to an increased rate of non-radiative recombination of the excited charge carriers. Therefore, under the same synthesis conditions, it is expected that as the synthesis temperature increases, the non-radiative recombination of the excited charge carriers within the quantum dots also increases and thus, the lifetime of the excited state typically decreases, as it is the case of Pd-doped $CsPbBr_3$. On the other hand, perovskite QDs face a chemical limitation due to their high volume-to-ratio, which results in a large number of uncoordinated atoms or ions on their surface. These surface defects act as traps for photogenerated excitons, leading to non-radiative recombination and quenching of the photophysical features. In the case of undoped $CsPbBr_3$ QDs, the lifetime may not decrease as significantly with increasing synthesis temperature as compared to doped perovskite quantum dots. This is because undoped perovskite quantum dots typically have fewer defects and impurities than doped perovskite quantum dots, which can act as non-radiative recombination centres for the excited charge carriers. At higher synthesis temperatures, the size of the undoped perovskite quantum dots increases, as is shown in Table 1, but this can actually lead to an increase in the lifetime of the quantum dots due to a decrease in surface area-to-volume ratio, which can

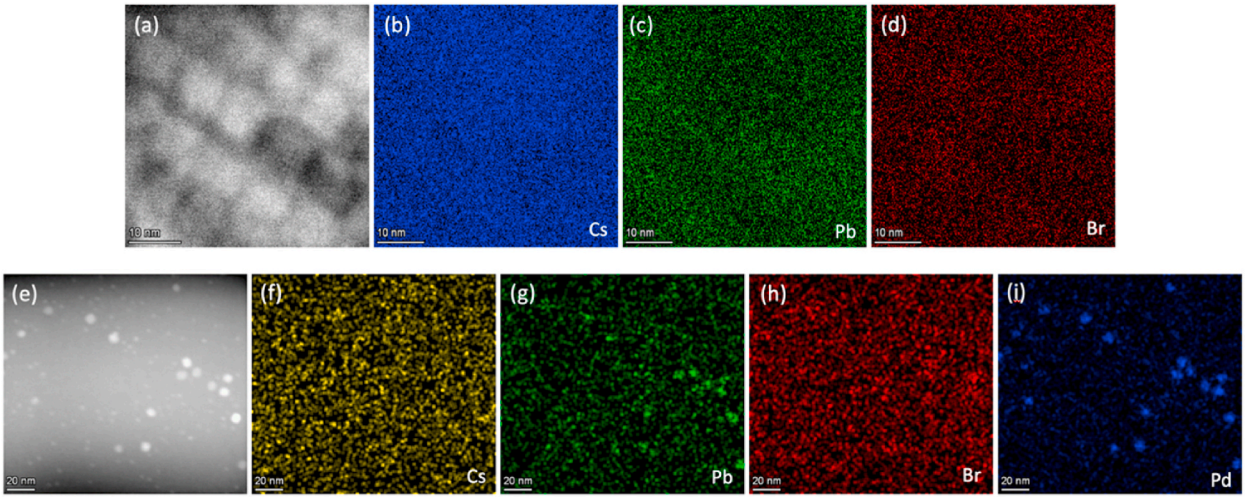

Fig. 6. HAADF-STEM image of $CsPbBr_3$ NCs (a) and the corresponding EDS elemental mapping images of Cs (b), Pb (c), and Br (d). HAADF-STEM image of the Pd-doped NCs (e) and the corresponding EDS elemental mapping images of Cs (f), Pb (g), Br (h) and Pd (i) elements. Bot samples were those synthesized at 130 °C in colloidal suspension.

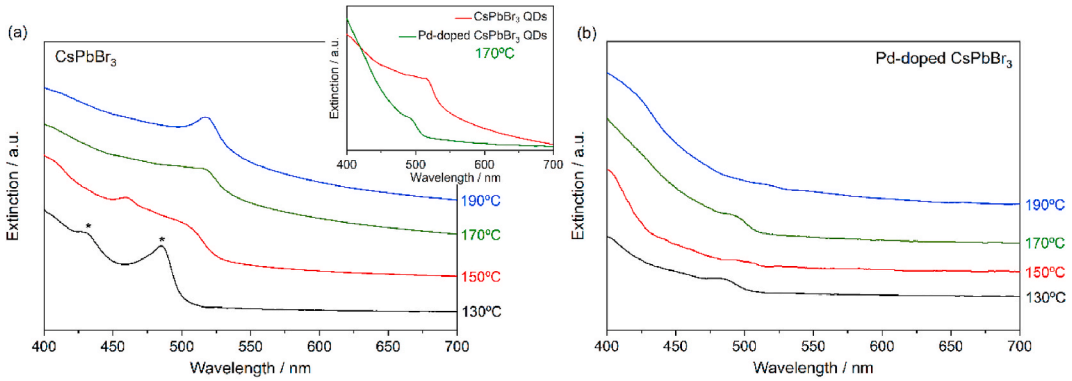

Fig. 7. UV–Vis spectra of the $CsPbBr_3$ (a), and Pd-doped $CsPbBr_3$ (b) perovskite NCs synthesized in colloidal suspension.

reduce the probability of surface trapping and non-radiative recombination.

3.2.7. Emission in the IR zone

The most remarkable result is the photoluminescence band at around 875 nm obtained under excitation at 785 nm for all the Pd-doped $CsPbBr_3$ NCs synthesized in colloidal suspension, presented in Fig. 10a, with a quantum yield of about 9.5%. This band was not observed in the undoped samples. Also, as the precursor $PbBr_2$ was kept in little amount in the bulk samples, PL measurements for $PbBr_2$ were performed by using the same excitation, and no emission was found. On the contrary, the undoped samples did not show any photoluminescence band. This is due to the interactions Pd–I, which affects to the band structure in Pd-doped perovskite. As was reported previously [19], the region of the valence band is clearly dominated by an overlap of the d states of the Pd with the p states of the I, which indicates the Pd–I interaction. That is, the d orbitals of the Pd in these perovskite-type structures provide empty and filled electron levels near to the edge of the valence band which makes the material behave in a similar way to a p-type semiconductor, with an optical band lower than undoped perovskite, which leads to a NIR emission. In addition, the stability of this NIR emission has been tested for several days. Fig. 10b shows the intensity of the emission, estimated as the area of the peak, up to 10 days after the synthesis for the Pd-doped $CsPbBr_3$ perovskite synthesized at 130 °C. A good stability of the emission is clearly observed. Thus, the Pd-doped samples could be applied in luminescent nanosensors as they meet one of the main conditions for this application: they are excited using a NIR laser and emit in any of the three biological windows (in this case, the first biological window) [31].

4. Conclusions

This paper presents the successful synthesis of $CsPbBr_3$ and Pd-doped $CsPbBr_3$ NCs synthesized in colloidal suspension using the hot-injection method at different synthesis temperatures. A SAED analysis from TEM images confirmed that, in both cases, the

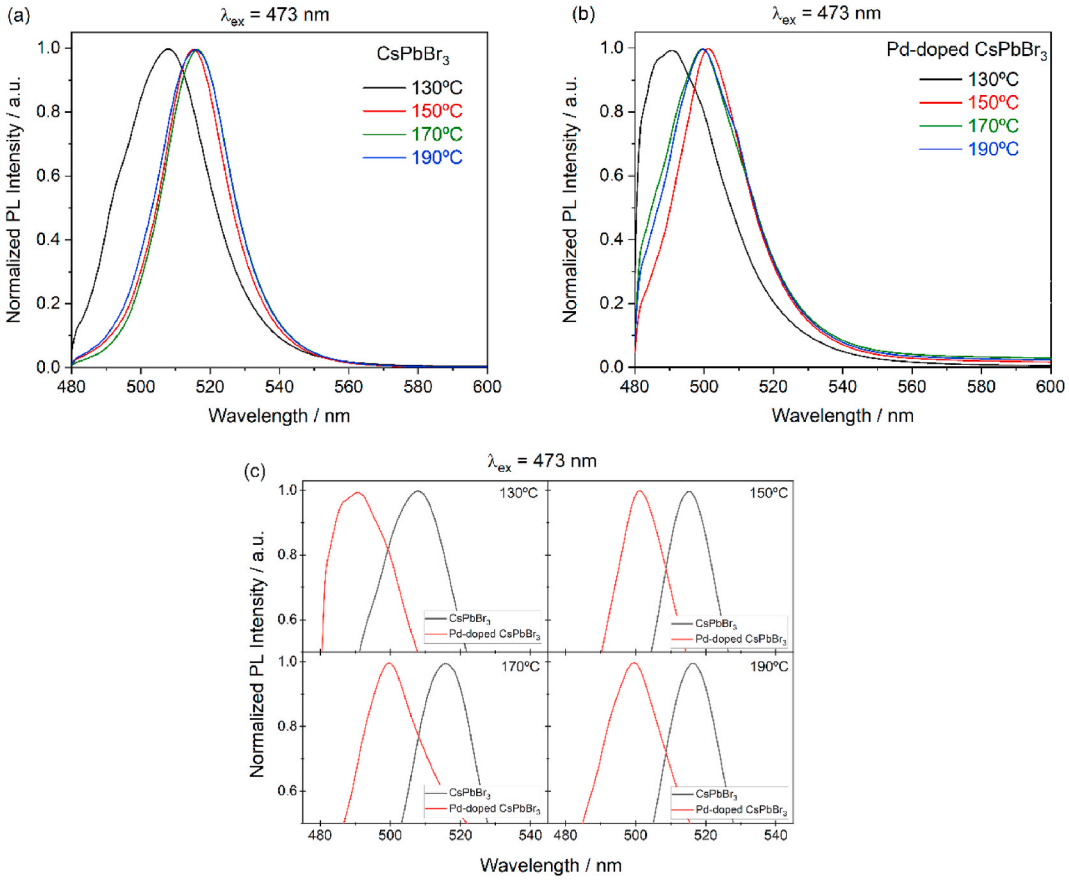

Fig. 8. Normalized PL spectra for $CsPbBr_3$ (a) and Pd-doped $CsPbBr_3$ (b) perovskite NCs, and comparison of the undoped and doped samples for each synthesis temperature (c).

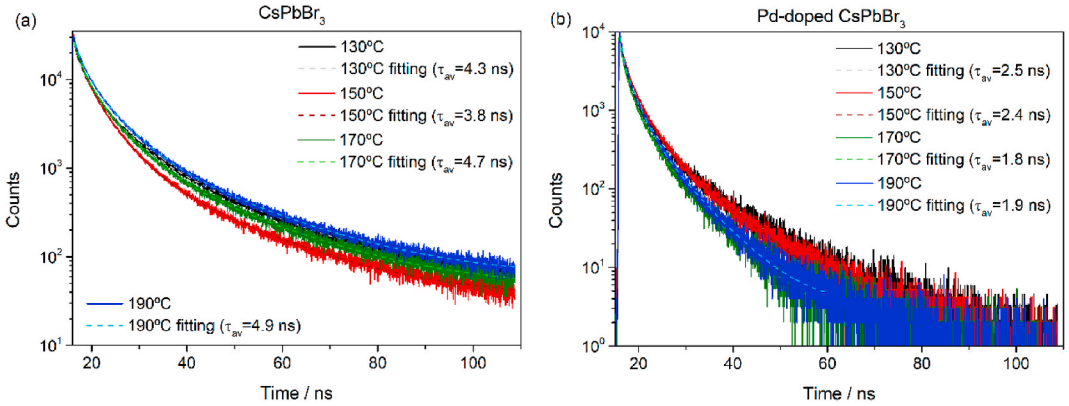

Fig. 9. Time-resolved PL decays and fitting curves for the undoped perovskite NCs (a) and Pd-doped NCs (b).

crystalline system is orthorhombic *Pnma*, which confirms the formation of a perovskite structure. The effect of the synthesis temperature and the Pd doping was studied through different techniques. This study shows that higher synthesis temperatures result in a gradual increase in the size of the nanoparticles, which produces a red-shift of the main PL band obtained under excitation at 473 nm. In addition, there is a blue-shift of the main emission band when perovskite nanocrystals are doped with Pd, and also of the absorption band. Nevertheless, the most remarkable result of this study was the fact that Pd-doped $CsPbBr_3$ NCs can be excited with a NIR laser emitting at 785 nm, and they emit in the NIR at about 875 nm. Therefore, they could be used to obtain luminescent nanothermometers, and in other applications related to biosensing, although further research is needed.

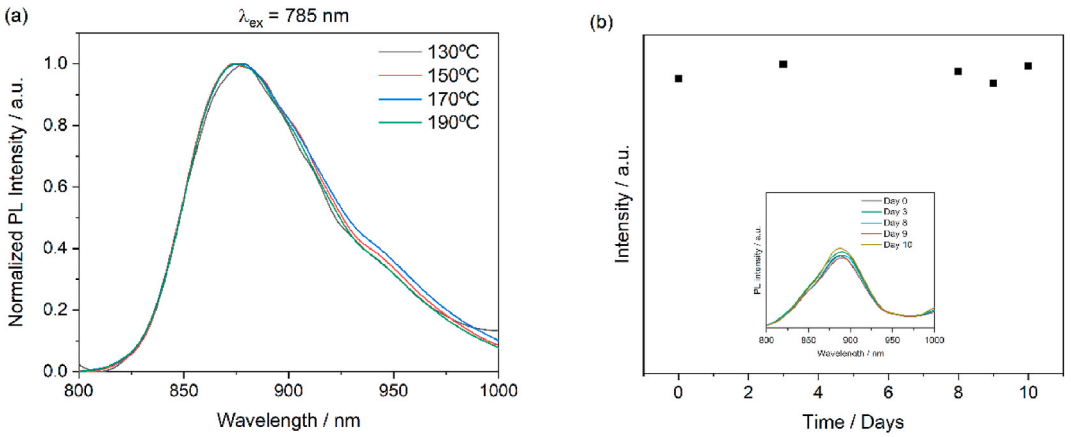

Fig. 10. (a) Normalized PL spectra of Pd-doped $CsPbBr_3$ perovskite NCs synthesized at different temperatures; and (b) stability analysis of the NIR emission for a Pd-doped $CsPbBr_3$ perovskite sample synthesized at 130 °C.

Author contribution statement

Mabel Rodríguez-Fernández: Performed the experiments; Contributed reagents, materials, analysis tools or data; Wrote the paper.
José Carlos Piñero: Performed the experiments; Contributed reagents, materials, analysis tools or data.
Rodrigo Alcántara: Analysed and interpreted the data.
Juan Jesús Gallardo: Performed the experiments.
Javier Navas: Conceived and designed the experiments.

Data availability statement

The authors do not have permission to share data.

Declaration of competing interest

The authors declare that they have no known competing financial interests or personal relationships that could have appeared to influence the work reported in this paper.

Acknowledgements

M.R.-F. acknowledges FPU19/02336 studentship from *Ministerio de Universidades del Gobierno de España*. This research was also funded by the Andalucía ERDF Operational Programme 2014–2020, managed by *Consejería de Transformación Económica, Industria, Conocimiento y Universidades de la Junta de Andalucía*, under grant FEDER-UCA18-107510. This work was also supported by *Ministerio de Ciencia e Innovación del Gobierno de España* [grant number TED2021-132518B–I00].

Appendix A. Supplementary data

Supplementary data to this article can be found online at https://doi.org/10.1016/j.heliyon.2023.e16775.

References

[1] C. Yan, C. Luo, W. Li, X. Peng, J. Cao, X. Zeng, Y. Gao, X. Fu, X. Chu, W. Deng, F. Chun, S. Yang, Q. Wang, W. Yang, Thermodynamics-induced injection enhanced deep-blue perovskite quantum dot LEDs, ACS Appl. Mater. Interfaces 13 (2021), 57560, https://doi.org/10.1021/acsami.1c16428.
[2] B. Xu, Z. Gao, S. Yang, H. Sun, L. Song, Y. Li, W. Zhang, X. Sun, Z. Wang, X. Wang, X. Meng, Multicolor random lasers based on perovskite quantum dots embedded in intrinsic Pb–MOFs, J. Phys. Chem. C 125 (2021), 25757, https://doi.org/10.1021/acs.jpcc.1c08362.
[3] S. Yan, Q. Li, X. Zhang, S. Tang, W. Lei, J. Chen, A vertical structure photodetector based on all-inorganic perovskite quantum dots, J. Soc. Inf. Disp. 28 (2020) 9, https://doi.org/10.1002/jsid.853.
[4] K.J. George, V.V. Halali, C.G. Sanjayan, V. Suvina, M. Sakar, R.G. Balakrishna, Perovskite nanomaterials as optical and electrochemical sensors, Inorg. Chem. Front. 7 (2020) 2702, https://doi.org/10.1039/d0qi00306a.
[5] J. Chen, D. Jia, E.M.J. Johansson, A. Hagfeldt, X. Zhang, Emerging perovskite quantum dot solar cells: feasible approaches to boost performance, Energy Environ. Sci. Adv. 14 (2020) 224, https://doi.org/10.1039/d0ee02900a.
[6] Y. Tu, J. Wu, G. Xu, X. Yang, R. Cai, Q. Gong, R. Zhu, W. Huang, Perovskite solar cells for space applications: progress and challenges, Adv. Mater. 33 (2021), 2006545, https://doi.org/10.1002/adma.202006545.

[7] Y.Q. Xu, Q. Chen, C.F. Zhang, R. Wang, H. Wu, X.Y. Zhang, G.C. Xing, W.W. Yu, X.Y. Wang, Y. Zhang, M. Xiao, Two-photon-pumped perovskite semiconductor nanocrystal lasers, J. Am. Chem. Soc. 138 (2016) 3761, https://doi.org/10.1021/jacs.5b12662.

[8] J.W. Choi, H.C. Woo, X. Huang, W.G. Jung, B.J. Kim, S.W. Jeon, S.Y. Yim, J.S. Lee, C.L. Lee, Organic-inorganic hybrid perovskite quantum dots with high PLQY and enhanced carrier mobility through crystallinity control by solvent engineering and solid-state ligand exchange, Nanoscale 10 (2018), 13356, https://doi.org/10.1039/c8nr00806j.

[9] G. Nedelcu, L. Protesescu, S. Yakunin, M.I. Bodnarchuk, M.J. Grotevent, M.V. Kovalenko, Fast anion-exchange in highly luminescent nanocrystals of cesium lead halide perovskites (CsPbX3, X = Cl, Br, I), Nano Lett. 15 (2015) 5635, https://doi.org/10.1021/acs.nanolett.5b02404.

[10] C.L. Li, Z.G. Zang, W.W. Chen, Z.P. Hu, X.S. Tang, W. Hu, K. Sun, X.M. Liu, W.M. Chen, Highly pure green light emission of perovskite CsPbBr3 quantum dots and their application for green light-emitting diodes, Opt Express 24 (2016), 15071, https://doi.org/10.1364/Oe.24.015071.

[11] C.L. Li, Z.G. Zang, C. Han, Z.P. Hu, X.S. Tang, J. Du, Y.X. Leng, K. Sun, Highly compact CsPbBr3 perovskite thin films decorated by ZnO nanoparticles for enhanced random lasing, Nano Energy 40 (2017) 195, https://doi.org/10.1016/j.nanoen.2017.08.013.

[12] B. del Rosal, E. Ximendes, U. Rocha, D. Jaque, In vivo luminescence nanothermometry: from materials to applications, Adv. Opt. Mater. 5 (2016), 1600508, https://doi.org/10.1002/adom.201600508.

[13] M. Runowski, N. Stopikowska, D. Szeremeta, S. Goderski, M. Skwierczyńska, S. Lis, Upconverting lanthanide fluoride Core@Shell nanorods for luminescent thermometry in the first and second biological windows: β-$NaYF_4$:Yb^{3+}– Er^{3+}@SiO_2 temperature sensor, ACS Appl. Mater. Interfaces 11 (2019) 13389–13396, https://doi.org/10.1021/acsami.9b00445.

[14] J. Navas, A. Sánchez-Coronilla, J.J. Gallardo, N.C. Hernández, J.C. Piñero, R. Alcántara, C. Fernández-Lorenzo, D.M. De los Santos, T. Aguilar, J. Martín-Calleja, New insights into organic–inorganic hybrid perovskite $CH_3NH_3PbI_3$ nanoparticles. An experimental and theoretical study of doping in Pb^{2+} sites with Sn^{2+}, Sr^{2+}, Cd^{2+} and Ca^{2+}, Nanoscale 7 (2015) 6216, https://doi.org/10.1039/c5nr00041f.

[15] J.J. Gallardo, M. Rodríguez-Fernández, E. Blanco, J. Outón, J. Navas, The effect of a complex A-site cation and mixed halides in the emission properties of perovskite quantum dots, J. Mol. Liq. 314 (2020), 113674, https://doi.org/10.1016/j.molliq.2020.113674.

[16] Y.X. Zhu, B.B. Yang, Q. Lu, L. Zhang, Y.R. Zhao, B.X. Xia, S.L. Mei, M.M. Shi, Y.F. Li, R.R. Hu, C.F. Guo, Y. Li, J. Zou, Stable Dy-doped CsPbBr3 quantum dot glass with enhanced optical performance, J. Non-Cryst. Solids 575 (2022), 121224, https://doi.org/10.1016/j.jnoncrysol.2021.121224.

[17] N. Ding, W. Xu, G.P.D. Zhou, D. Li, Y. Ji, X. Chen, D. Yang, X. Bai, C.-G. Ma, H. Son, Upconversion ladder enabled super-sensitive narrowband near-infrared photodetectors based on rare earth doped florine perovskite nanocrystals, Nano Energy 76 (2020), 105103, https://doi.org/10.1016/j.nanoen.2020.105103.

[18] W.X.N. Ding, D. Zhou, Y. Ji, Y. Wang, R. Sun, X. Bai, J. Zhou, H. Song, Extremely efficient quantum-cutting Cr3+, Ce3+, Yb3+ tridoped perovskite quantum dots for highly enhancing the ultraviolet response of Silicon photodetectors with external quantum efficiency exceeding 70%, Nano Energy 78 (2020), 105278 https://doi.org/10.1016/j.nanoen.2020.105278.

[19] Z.M. Zhang, M.M. Wang, Y.R. Liu, J.C. Zhang, J. Wang, J.J. Han, C. Liu, J. Ruan, Long-term stable and highly efficient photoluminescence from Sr2+-doped CsPbBr3 nanocrystals in boro-germanosilicate glass, Ceram. Int. 48 (2022), 17596, https://doi.org/10.1016/j.ceramint.2022.03.029.

[20] N. Ding, Y. Wu, W. Xu, J. Lyu, Y. Wang, L. Zi, L. Shao, R. Sun, N. Wang, S. Liu, D. Zhou, X. Bai, J. Zhou, H. Song, A novel approach for designing ef!cient broadband photodetectors expanding from deep ultraviolet to near infrared, Light Sci. Appl. 11 (2022) 91, https://doi.org/10.1038/s41377-022-00777-w.

[21] Y. Yang, Y. Li, W. Gong, H. Guo, X. Niu, Cobalt-doped CsPbBr3 perovskite quantum dots for photoelectrocatalytic hydrogen production via efficient charge transport, Colloids Surf. A Physicochem. Eng. Asp. 663 (2023), 131083, https://doi.org/10.1016/j.colsurfa.2023.131083.

[22] J. Navas, A. Sánchez-Coronilla, J.J. Gallardo, J.C. Piñero, D. De los Santos, E.I. Martín, N.C. Hernández, R. Alcántara, C. Fernández-Lorenzo, J. Martín-Calleja, The impact of Pd on the light harvesting in hybrid organic-inorganic perovskite for solar cells, Nano Energy 34 (2017) 141, https://doi.org/10.1016/j.nanoen.2017.02.035.

[23] B. Zhang, K. Zhang, L. Li, C. Xu, R. Wang, C. Wang, J. Yang, Y. Yang, J. Wang, F. Qiu, T. Sun, C. Zhou, X. Wen, Enhancing stability and luminescence quantum yield of $CsPbBr_3$ quantum dots by embedded in borosilicate glass, J. Alloys Compd. 874 (2021), 159962, https://doi.org/10.1016/j.jallcom.2021.159962.

[24] W.W. Chen, X. Xin, Z.G. Zang, X.S. Tang, C.L. Li, W. Hu, M. Zhou, J. Du, Tunable photoluminescence of $CsPbBr_3$ perovskite quantum dots for light emitting diodes application, J. Solid State Chem. 255 (2017) 115, https://doi.org/10.1016/j.jssc.2017.06.006.

[25] J. Ding, S. Du, Z. Zuo, Y. Zhao, H. Cui, X. Zhan, High detectivity and rapid response in perovskite $CsPbBr_3$ single-crystal photodetector, J. Phys. Chem. Lett. 121 (2017) 4917–4923, https://doi.org/10.1021/acs.jpcc.7b01171.

[26] L. Protesescu, S. Yakunin, M.I. Bodnarchuk, F. Krieg, R. Caputo, C.H. Hendon, R.X. Yang, A. Walsh, M.V. Kovalenko, Nanocrystals of cesium lead halide perovskites (CsPbX3, X = Cl, Br, and I): novel optoelectronic materials showing Bright emission with wide color gamut, Nano Lett. 15 (2015) 3692, https://doi.org/10.1021/nl5048779.

[27] J.-H. Cha, J.H. Han, W. Yin, C. Park, Y. Park, T.K. Ahn, J.H. Cho, D.-Y. Jung, Photoresponse of $CsPbBr_3$ and Cs_4PbBr_6 perovskite single crystals, J. Phys. Chem. Lett. 8 (2017) 565, https://doi.org/10.1021/acs.jpclett.6b02763.

[28] X. Zhang, F. Wang, B.-B. Zhang, G. Zha, W. Jie, Ferroelastic domains in a $CsPbBr_3$ single crystal and their phase transition characteristics: an in situ TEM study, Cryst. Growth Des. 20 (2020) 4585, https://doi.org/10.1021/acs.cgd.0c00370.

[29] P.D. Nellist, S.J. Pennycook, The principles and interpretation of annular dark-field Z-contrast imaging, Adv. Imag. Electron. Phys. 113 (2000) 147, https://doi.org/10.1016/S1076-5670(00)80013-0.

[30] P. Cottingham, R.L. Brutchey, On the crystal structure of colloidally prepared $CsPbBr_3$ quantum dots, Chem. Commun. 52 (2016) 5246, https://doi.org/10.1039/c6cc01088a.

[31] D. Jaque, F. Vetrone, Luminescence nanothermometry, Nanoscale 4 (2012) 4301, https://doi.org/10.1039/C2NR30764B.